January 1996

Dynamic phenomena in organic metal (BEDT-TTF)3Ta2F11

Juana Acrivos
San Jose State University, juana.acrivos@sjsu.edu

37

Dynamic phenomena in superconducting organic metals by ESR

Juana Vivó Acrivos,* and Lei Chen, San José State University, San José CA 95192-0101

Abstract:

Dynamic electron spin resonance, ESR measurements suggest that $(BEDT\text{-}TTF)_3Ta_2F_{11}$ a paramagnetic, layer, organic metal, has similar properties as cuprate superconductors. The response to microwave radiation in a modulated external magnetic field indicates: (i) there is a condensation of free spin doublet to triplet states below T_{00}=150±10K; (ii) T_{00} is above the transition temperature to superconductivity T_c=10±1 K (detected by the onset of an energy loss at exactly H=0) because (iii) antiferromagnetic AF resonance is observed down to 85 K; (iv) the relaxation time τ_1 for the half field, triplet state ESR absorption increases fourfold near 10 K and, (v) the onset of superconductivity is also detected by the appearance of magnetization oscillations below T_c when the sample is cooled in a non-zero filed H. Near 150 K the exchange field between the aligned AF domains (ascertained from the AF resonance orientation field dependence) J_{AF} =130 mT (10^2 mK) is greater than the exchange term J≈ 15 mT (13 mK) between free spins, S=1/2 (estimated from the g=2 line shapes). The presence of AF domains below 150 K is assumed to be the reason why the superconducting transition is observed only below 10 K. The spin-lattice relaxation time for the triplet state half field ESR near 10 K is interpreted using the Gorter phenomenological relation $\tau_1=C_H/\alpha_H$, C_H and α_H are respectively the heat capacity and the thermal contact coefficient to the bath of the spin system, at constant field H.

* To whom all correspondence should be sent
PACS Numbers: 76.30.-v; 74.25.Nf; 74.40.+k; 74.50.+r;

Introduction:

Some of the most accurate methods used to determine the transition temperature T_c to the superconducting state (in addition to transport measurements) are based on the thermodynamics of the phase transition, i.e., the jump in the heat capacity; and others that are directly associated with this thermodynamic property such as the nuclear magnetic resonance, NMR spin-lattice relaxation time of nuclei in hyperfine contact with the Bose condensate.[1] The value of T_c can also be ascertained by the appearance of an energy loss at exactly zero field.[2,3] The transition to superconductivity of the paramagnetic organic metal $(BEDT\text{-}TTF)_3Ta_2F_{11}$,[4] is ascertained in this work from the onset of the energy loss near H=0 and magnetization jumps observed when the samples are cooled below T_c in $H\neq 0$ and, the relaxation time τ_1 which is related to the thermodynamic parameters by the Gorter,[5] relation:

$$\tau_1 = C_H/\alpha_H, \quad (1)$$

where C_H and α_H are respectively the heat capacity and the coefficient of thermal contact of the spin system (at temperature T_S) to the lattice (at temperature T_0) at constant field H and, the spin temperature changes with time as:

$$dT_S/dt = (T_0-T_S)/\tau_1, \text{ when } |T_0-T_S|/T_0 \ll 1. \quad (2)$$

The paramagnetic layer organic metal $(BEDT\text{-}TTF)_3Ta_2F_{11}$ (figure 1a) consists of anion acceptor layers $Ta_2F_{11}^-$ and of donor layers where the $((CH_2)_2S_2C_2S_2C{=}CS_2C_2S_2(CH_2)_2)_3^+$ free

radical cations (S=1/2) are aligned 20° from the c-axis to maximize the chalcogen, π-π intermolecular interactions. ESR measurements have already given information on the chemical dynamics that the free radical undergoes as a function of temperature (figure 1b).[4a] The change in the inverse temperature dependence of the line width $\Delta B_{z,ms}$ for the g=2.00 doublet D, and the appearance of triplet state T* indicate that new phenomena are present below the temperature T_{00} = 150±10K. A transition below 7 K was ascertained earlier from the broadening of the D and T* ESR near g=2. A charged free spin species interacting with the lattice vibrations produces the polarization called a polaron.[6] Mott, and Alaxandrov and Mott,[6c] have shown that such charged carriers with spin S=1/2 in a many-electron system, when they are strongly coupled to the lattice vibrations, can tunnel to form a charged Bose-liquid of small bipolarons with charge 2e and S= 0 or 1. The purpose of this work is to apply the Alexandrov and Mott theory to $(BEDT\text{-}TTF)_3Ta_2F_{11}$, in order to understand the transition near T_{00} and, to ascertain the transition to superconductivity by applying the Gorter relation (1) to the half field T* ESR lattice relaxation times, i.e., the Gorter phenomenological relation may be applied to the ESR of the carriers directly responsible for the transition to superconductivity in the same manner that the beautiful NMR work applied the BCS theory to cuprate superconductors using the relaxation times of fixed nuclei in hyperfine contact with the condensate.[1b,c] In the thermodynamic, phenomenological description the important parameters in the transition to superconductivity are the jump in the heat capacity and, in the thermal contact coefficient near T_c; thus τ_1 measurements for the T* ESR may be able to ascertain whether the triplet state of the condensate is directly involved in the transition to superconductivity.

Experimental:

The 10 mg oriented single crystal of $(BEDT\text{-}TTF)_3Ta_2F_{11}$ (figure 1a) was prepared at IBM;[4b] the x-band Bruker-ER300/Oxford-900 spectrometer/cryogenic system used for the measurements was described earlier.[2,4a] Figures 2a-d show the power absorption derivative dP/dB_z response to the field $\mathbf{k}(B_z+2B_{zm}\cos(2\pi\nu_m))+2\mathbf{i}B_1\cos(2\pi\nu)$ with ν=9.36Ghz, $\nu_m=10^5$Hz, $B_1=B_{10}E\text{-}dB/20$, $B_{10}\leq 0.1$mT, versus B_z and temperature T from 280 K down to 3.7 K when $B_1\|a\perp B_z\wedge b=\theta$: near zero field (energy loss in the superconducting state exactly at H = 0,[2,3]) ESR near g=2.00 (D and T*, $\Delta S_z=\pm 1$) and, near the half field resonance (T*, $\Delta S=0$), antiferromagnetic AF resonance,[2] and magnetization oscillations,[7] when $T<T_c$ if the sample is cooled in $H\neq 0$. For comparison figure 3 shows the ESR of a 1 mg $YBa_2Cu_3O_7\text{-}\delta$ (T_c=85 K) prepared by C.T. Lin at the IRC for Superconductivity, Cambridge, UK.[8]

Results and Discussion:

Four types of response (figure 2) are identified by their orientation dependence in the external magnetic field as described in the Appendix:[2,4,5b] (i) The ESR fields $B_{z,i}$ (figure 2a) for doublet and triplet states depend on the photon energy $h\nu$ and the crystal orientation in the external field. The important parameters for the discussion are the g factors (g_{xx},g_{yy},g_{zz})=(2.0125,2.0030,2.0023) obtained from relations (A1) for the D states as well as the temperature dependence of the line shapes reported earlier (figure 1b).[4] Figure 2d shows the reversible change in the D ESR line shape; near the center, the lines are as sharp as above T_{00} but, the amplitude in the wings is greater below T_{00}. The Anderson and Weiss theory,[5b,c] is applied to explain the line shape below T_{00} in the Appendix, and to obtain an exchange field

$J \approx 15$mT. The T*, $\Delta S=0$ transition saturates faster than the D, $\Delta S_z=\pm 1$ (figures 2a,c,d). The spin-lattice relaxation times (figure 4a) are measured by saturation experiments using relation (A4).[5b] (ii) AF resonance at fields $B_{z,i}$ (figure 2b) depend on the photon energy $h\nu$, the crystal orientation in the external field relative to the direction of the anisotropy field B_A produced in the different AF domains.[2] The important parameters obtained from the orientation dependence (figure 4b) using relation (A2) are the anisotropy field i $B_A=220$ mT, and the field produced by the exchange interaction between spins in the different domains, [5d] $B_E= 130$ mT$=J_{AF} = 10^2$ mK and $g = 1.74$, correct to 10% accuracy. (iii) The onset of the energy loss at exactly H=0 (figure 2a) identifies T_c,[2,3] by the appearance of a signal of opposite polarity to the ESR near $T_c=10\pm 1$ K. (iv) Another signature of superconductivity observed is the appearance of magnetization jumps (due to flux pinning) when the crystal is cooled in $H\neq 0$ through T_c,[7]; these disappear when the sample is cooled through T_c in exactly zero field (figure 2a). The onset of the latter two responses have been used in the literature to identify the transition to superconductivity at T_c for metal superconductors.[3,7] The sharp ESR absorptions (figure 2) now alllow the measurement of spin relaxation times vs T.

The fourfold increase in τ_1 (figure 4a) occurs near the same temperature as the onset of an energy loss signal at H=0 and, magnetization oscillations when the crystal is cooled in $H\neq 0$; it may be used to relate τ_1 to T_c using the Gorter phenomenological relation (1) and the rate processes between the states in figure 5: There are five spin states split by the field ($B_{z,½}\approx 156$ mT) in dynamic equilibrium: two D states ($|1/2\pm 1/2\rangle$) and three T* states ($|1,\pm 1\rangle$ and $|1,0\rangle$) with the corresponding level population $n_{|S,Sz\rangle}$ if at temperature T_S and $N_{|S,\,Sz\rangle}$ if at thermal equilibrium with the lattice and the radiation bath at temperature T_0 in Table I. The ground state

is a singlet S in equilibrium with the D states and the latter are in equilibrium with the T* states via the chemical reactions:

$S \Leftrightarrow 2D$ and $2D \Leftrightarrow T^*$, (3)

with equilibrium constants:

$K_2 = (a[D])^2/a[S] = \exp(-\Delta_{S\text{-}D}/2T)$,

$K_3 = k_1/k_{-1} = a[T^*]/(a[D])^2 = \exp(\Delta_{T^*\text{-}D}/2T)$, (4)

the doublet lies above the ground state by $\Delta_{S\text{-}D}/2 = 3E{+}3$ K at room temperature decreasing to 30 K near T_c and the triplet state lies below the doublet by $\Delta_{T^*\text{-}D}/2 \rightarrow \pm 0$ as $T \rightarrow T_c$. The activities a[i] were ascertained from D, T* $\Delta S_z = \pm 1$ ESR intensity measurements, in the absence of saturation above T_c, assuming $a[S] \cong 1$ is the standard state.[4a] The rate constant k_1 was determined previously from the line width broadening of the D, $\Delta S_z = \pm 1$ ESR vs 1/T (figure 1b) as:

$\Delta B_{z,ms} = \text{constant}(k_1 + 1/T_2)$,

$k_1 = A_0\, e^{\Delta S/R}\, e^{-\Delta U/RT}$, (5)

where $(\Delta U/R,\ A_0 e^{\Delta S/R}) = (111\text{ K},\ 3.5*10^7/s)_{T > T_{00}}$; $(11\text{ K},\ 7*10^6/s)_{T<T_{00}}$ when ΔU and ΔS are respectively the activation energy and entropy to form the activated states leading to the disappearance of D. The decrease in ΔU below T_{00} indicates that there is an easier path for the disappearance of D whereas the entropy increase, by $\approx 2R$ above T_{00}, suggests that disorder is

introduced by the two possible spin flips for each of the three singlet states formed by antiparallel pairing (above T_{00}) along each of the principal axes of triplet state formation (X_T,Y_T,Z_T, in figure 1a), each contributing Rℓn2 to the entropy, i.e., the triplet states do not provide a relaxation path above T_{00}. Tunneling of D polarons via lattice vibrations pair the spins as S* states with 1/4 probability and T* states with 3/4 probability. The separation between the individual bands (figure 5) is determined by the equilibrium constatns (4). All the dynamic phenomena depend on the lattice vibrations, e.g., the population and rates of disappearance and formation of the D, S* and T* states depend on the coupling of spins to the lattice vibrations. The spin system S (with components separated in energy by ΔE) satisfy the Boltzmann population distribution, e.g., $n_{|S,Sz>}/n_{|S,-Sz>} = \exp -\Delta E / k_B T_S$; in a saturation experment the system temperature T_S is greater than the bath temperature T_0 and thermal equilibrium is obtained when the Boltzmann temperature approaches T_0; the chemical rates, the spin-spin and spin-lattice, and spin-radiation interactions determine the relaxation rates $w(\Delta E)$ between the spin states separated by ΔE in figure 5. It has been shown that the most efficient processes involve resonant phonons produced via second order Raman processes,[5b] i.e., the absorption and emission of phonons at frequencies ν_1 and ν_2 respectively when $\nu_1 - \nu_2 = \nu$, e.g.,

$$E_{|S,Sz>} + h\nu_{radiation} = E_{|S,-Sz>};\ E_{|S,-Sz>} + h\nu_{phonon1} = E_{intermediate};\ E_{intermediate} - h\nu_{phonon2} = E_{|S,Sz>}. \quad (6)$$

The phonons are at temperature T_{phonon} with heat capacity C_{phonon}; they are in contact with the lattice at temperature T_0 and infinite heat capacity, and the transition probabilities $w(\Delta E)$ depend on the energy transfer path:

Spin System (T_S, C_H)⇒Resonant Phonons (T_{phonon}, C_{phonon})⇒Bath (T_0, Infinite Heat Capacity)

and since $C_{phonon} < C_H$ there is a bottleneck when the phonons are involved in phase transitions. The magnetization relations in the Appendix (A6) obtain the relaxation time for the T*(ΔS=0) transition:

$$\tau_1(h\nu) = [w^{=}(h\nu)+w^{++}(h\nu)) + (w^{-}(h\nu/2)+w^{+}(h\nu/2))/2 \quad + k_{-1}]^{-1}, \qquad (7)$$

i.e., the fourfold τ_1 increase near 10 K suggests that a phonon bottleneck decreases the rates $w(\Delta E)$ and that the lifetime of T* is determined by $1/k_{-1}$, which also depends on the lattice vibrations. In order to associate T_c with the τ_1 jump and the Gorter relation (1):

$$\Delta(\tau_1,T_c)/\tau_1 = \Delta C_H/C_H \; - \Delta\alpha_H/\alpha_H \approx 4,$$

the data must be compared with heat capacity C_p taken together with thermal conduction coefficients K near T_c where C_H and α are the electronic contributions of the spin system to the latter); Cp and K are known accurately for cuprate superconductors;[1] $\Delta C_p(T_c)/C_p \cong 0.03$, $\Delta K(T<T_c)/K = 0.3$,[1d,e] for $YBa_2Cu_3O_{7-\delta}$ but the authors estimate that the electronic contributions are $\Delta C_e(T_c)/C_e \cong \Delta K_e(T<T_c)/K_e = 3$ to 4 , suggesting that the fractional increase in C_e and in α are of the same order of magnitude but that α increases well below T_c. If the latter applies also to organic superconductors, an increase in α below T_c would lead to the τ_1 decrease in figure 4a.

Other similarities between the organic and the cuprate superconductors may be obtained

from the single crystal ESR (figure 3); the T* half field ESR absorption by a single crystal $YBa_2Cu_3O_{7-\delta}$ (T_c=85 K)[8] observed below T_c (cooled in H =0 and in H≠0) and the absence of D ESR below T_c suggests that k_1 is shorter than 10^{-10} s. If bipolarons are formed by the π-π intermolecular interactions along the triplet axes in the organic conductor, the activation energy ΔU for the tunneling interactions will be inversely proportional to the corresponding S-S bond order (10^{-3})[9] then if bipolarons are formed in cuprate superconductors by O-O polarization interactions in the CuO_2 plane, the bond order for diagonal sigma bonded O-O pairs (10^{-2} for $<r_{oo}>\cong 0.27$nm)[10] suggests that ΔU is an order of magnitude smaller for the latter. Also if the T* gap states contribute to the transport properties then as $1/2\Delta_{S\text{-}D} \rightarrow J$ as $T \rightarrow 0$ K, it should be evident in the dependence of such transport properties as the Hall coefficient vs T, as it is in superconducting cuprates.[11]

The competition between AF and superconductivity in the organic layer superconductor appears to be similar to that found in superconducting oxides.[2] The AF resonance line width increases as T decreases below 150 K (figure 2b), indicating that the domain lifetime lifetime decreases to a temperature which allows the appearance of superconductivity at T_c i.e, the exchange fields measured near 150 K, J_{AF} = 130 mT > J ≈15 mT suggest that at this temperatures superconductivity is not allowed by the presence of AF domains in the single crystal, however as the lifetime of the latter decreases below 10^{-10} s, the superconducting transition is allowed.

The decrease in the bipolaron binding energy $\Delta_{S\text{-}D}/2$ (figure 5) with T suggests that it may continue to decrease down to $T \rightarrow J \approx 15$ mT (13 mK). This will also depend strongly on the lattice vibrations.

Conclusions:

The change in the D, ESR line shape and the appearance of the T*, $\Delta S=0$ ESR identifies the transition temperature where the pairing of doublet polaron states produce a triplet condensate in the organic metal near $T_{00}=150\pm10K$. This is of some importance for any theory of superconductivity which predicts the formation of a Bose condensate above $T_c = 10\pm$ K.[5b] The fact that the T*, $\Delta S=0$ ESR saturates faster than the D with a large increase in τ_1 near T_c suggests that the former are part of the superconducting condensate because they appear to be more sensitive to the changes in the electronic heat capacity at the transition.

Acknowledgements:

This work was carried out at SJSU with support from NSF grants DMR 9307387 and INT 9312176. JVA is grateful to Alexandrov and Mott. The work is dedicated to JVA's first mentor John E. Wertz, who introduced her to Gorter's phenomenological relations.

References:

1. (a) D.M. Ginsberg, **"Physical Properties of High Temperature Superconductors, I"**, *D.M. Ginsberg, ed.*, World Scientific, New Jersey (1989), p. 1; (b) L.C. Hebel and C.P. Slichter, *Phys. Rev.* **113**, 1504 (1959); (c) C.H. Pennington and C.P. Slichter, **"Physical Properties of High Temperature Superconductors, II"**, *D.M. Ginsberg, ed.*, World Scientific, New Jersey (1990), p. 269; (d) M.B. Salamon, S.E. Inderhees, J.P. Rice, B.G. Paxol, D.M. Ginsberg and N. Goldenfeld, *Phys. Rev. B* **38**, 885 (1988) ; (e) C. Uher and A.B. Kaiser, *Phys. Rev. B* **36**, 5680 (1987)

2. J.V. Acrivos, Lei Chen, P. Metcalf, J.M. Honig, R.S. Liu and K.K. Singh, *Phys. Rev. B*, **50**, 13710 (1994)

3. F. G. Adrian and D. O. Cowan, *Chem. and Eng. News*, **70**, 40 (1992)

4.(a) J.V.(Vivo') Acrivos, P. Hughes and S.S.P. Parkin, *J. Chem. Phys.* **86**, 1780 (1987); (b) S.S.P. Parkin, E.M. Engler, V.Y. Lee and R. Schumaker, *Mol. Liq. Cryst.***119**, 375 (1985)

5. (a) C.J. Gorter, **"Paramagnetic Relaxation"**, Elsevier Publishing Company, Inc. Amsterdam (1947); (b) A. Abragam and B. Bleaney, **"Electron Paramagnetic Resonance of Transition Ions"**, Clarendon Press, Oxford (1970); (c) P.W. Anderson and P.R. Weiss, *Rev. Mod. Phys.* **25**, 269 (1953)

6. (a) H. Frölich,**"Polarons and Excitons"**, p. 1, *C.G. Kuper and G.D. Whitfield ed.*, Plenum Press, N.Y. 1963; (b) D. Pines, *ibid.*, p.33; (c) A.S. Alexandrov and N.F. Mott, *International Journal of Modern Physics B* **8**, 2075-2109 (1994)

7.(a) J.L. Tholence, H. Noel, J.C. Levet, M.Potel and P.Gugeon, *Solid State Communications*,. **65**, 1131 (1988); (b) H.R. Brand, and mauro M. Doria, *Phys. Rev. B*, **37**, 9722 (1988)

8. C.T. Lin, W. Zhou and W.Y. Liang, *Physica C* **195**, 291 (1992)

9. Lei Chen, MS Thesis, SJSU (1987)

10. J.V. Acrivos and O. Stradella, *Int. J. of Quantum Mechanics* **46**, 55 (1993)

11. A.P. Mackenzie, S.R. Julian, G.C. Lonzarich, A. Carrington, S.V. Brown and D.C. Sinclair, *Phys. Rev. Lett.* , **71**, 1238 (1993)

List of Figures:

Figure 1: $(BEDT\text{-}TTF)_3Ta_2F_{11}$, crystallographic axes: a=1.6683, b=1.1928, c=1.255nm (a) Structure according to ref. 4b. (b) Temperature dependence of the doublet D ESR absorption line width between the points of maximum slope $\Delta B_{z,ms}$, according to ref. 4a.

Figure 2: $(BEDT\text{-}TTF)_3Ta_2F_{11}$ $B_Z \perp B_1 \| a\text{-axis}$, $\theta = b \wedge B_z$, dP/dB_z vs B_z response to the field: (a) Resonance fields satisfying relations (A1) to (A4); energy loss and magnetization oscillations near 3.7 K for sample cooled through T_c in non-zero field (due to flux pinning with a periods of 10^0 mT (near $B_z \approx 10^2$ mT) to 100 mT (near $B_z \approx 1$ tesla)) , these disappear when the sample is cooled in zero field through T_c. (b) T dependence of low field AF resonance and appearance of T*, $\Delta S=0$ ESR absorbtion near T_{00}. $T < T_c$: (c) Saturation experiments with the gain normalized to the increase in B_1. The saturation factor is given by relation (A5). These show that neither the energy loss nor the magnetization oscillations depend on the incident power and that the T* saturates faster than the D ESR. (d) D, ESR absorption near T_{00} showing changes in line shape.

Figure 3: Half field T* ESR for $YBa_2Cu_3O_{7-\delta}$ below T_c (cooled in $H = 0$ and in $H \neq 0$)

Figure 4: $(BEDT\text{-}TTF)_3Ta_2F_{11}$: (a) T*, $\Delta S=0$ spin-lattice relaxation time τ_1 vs T, evaluated by cw saturation experiments. (b) AF resonance field $B_{z,AF}$ vs angle $\theta = b \wedge B_z$: ♦, experimental field; □, calclated field using relation (A3) and ▲, the absolute deviation.

Figure 5: $(BEDT\text{-}TTF)_3Ta_2F_{11}$: Energy level diagram near $B_{z,1/2}$. The insert shows the equilibrium constants the formation of D and T* vs T from ref. 4a. The double arrows indicate energy level separation whereas the single arrows point to a relaxation process.

Table I: dn_i/dt subject to the irradiation of the T*, $\Delta S=0$ transition and chemical rates:[a,b,c]

$$dn_{|1,-1>}/dt = -(w^{++}+k_{-1}+w^{+})n_{|1,-1>} + w^{-} n_{|1,0>} + w^{=} n_{|1,1>} + k_1(n_{|1/2,-1/2>})^2$$

$$dn_{|1,0>}/dt = w^{+}n_{|1,-1>} -(w^{+} + w^{-}+ k_{-1})n_{|1,0>}+ w^{-} n_{|1,1>} + k_1 n_{|1/2,-1/2>} n_{|1/2,1/2>}$$

$$dn_{|1,1>}/dt = w^{++} n_{|1,-1>} + w^{+} n_{|1,0>} -(w^{=} +k_{-1}+w^{-})n_{|1,1>} + k_1(n_{|1/2,1/2>})^2$$

$$dn_{|1/2,-1/2>}/dt=2k_{-1}(n_{|1,-1>}+N_{S*})-w^{+}n_{|1/2,-1/2>}+w^{-}n_{|1/2,1/2>}- 2\,k_1\, n_{|1/2,-1/2>}(n_{|1/2,-1/2>}+n_{|1/2,1/2>})$$

$$dn_{|1/2,1/2>}/dt=2k_{-1}(n_{|1,1>}+N_{S*})-w^{-}n_{|1/2,1/2>}+w^{+}n_{|1/2,-1/2>}- 2\,k_1\, n_{|1/2,1/2>}(n_{|1/2,1/2>}+n_{|1/2,-1/2>})$$

a. $dn_i/dt = 0$ at steady state equilibrium, at T_0 requires:

$$w^{++}-w^{=}\exp(-h\nu/k_BT_0) = w^{+}-w^{-}\exp(-h\nu/2k_BT_0) = 0$$

b. Assuming that the non saturated levels are at T_0:

$$n_{|1,0>} \rightarrow N_{|1,0>},\quad n_{|1/2,1/2>} \rightarrow N_{|1/2,-1/2>},\quad n_{|1/2,1/2>} \rightarrow N_{|1/2,1/2>}$$

obtains, correct to first order in the Curie-Weiss regime:

$$dn_{|1,0>}/dt = w^{+}(h\nu/2k_BT_s)^2(T_0-T_s)/T_0 + k_{-1}(N_{|1,0>}-n_{|1,0>}) \approx 0$$

or,

$$w^{+} n_{|1/2,-1/2>} = w^{-} n_{|1/2,1/2>}.$$

Appendix

The spectroscopic identification of the magnetic response uses the principles of magnetic resonance:[5] ESR occurs at resonance fields $B_{z,i}$ given by:[2,4,5b]

$$h\nu = 2\sqrt{(G_{T^*,0}^2+E^2)}_{B\|a} = G_{T^*,\pm1} = G_{D,\pm1}, \quad (A1)$$

$G_{T^*,0}=g_{T^*}\beta B_{z,T^*1/2}$, $G_{D,\pm1}=g_D\beta B_{z,D}$, $G_{T^*,\pm1}=g_{T^*}\beta B_{z,T^*1} \pm\{D(3\cos^2\theta-1)+E\sin^2\beta\cos2\phi\}+O^2$, E,D are components of an axial, triplet fine structure tensor at angles β,ϕ to B_Z. The D and T* $g_{x,y,z}=2.00$, $\Delta S_z=\pm1$ transitions in a rhombic crystal field have been described previously.[4] The orientation independent, sharp T*, $\Delta S=0$ half field ESR transition appears below $T_{00}=150$ K (figure 2b), its transition probability is $\approx 2(E/G_{T^*,0})^2$ relative to the T*, $\Delta S_z=\pm1$ when $B_z\|B_1\|a$.[5b] The observed resonance intensity near $B_{z,1/2}$ is an order of magnitude weaker than the D, g=2, $\Delta S_z=\pm1$ intensity at ≈ 150 K; this may be compared to the expected intensity $2(E/G_{T^*,0})^2 \approx 2(B_{z,D}-2B_{z,1/2})/B_{z,1/2} \approx 0.24$ for the laboratory configuration $B_z\|B_1\|a$, here the half field transition is allowed because $B_z \perp B_1$ is not parallel to any of the triplet axes. AF resonances with axial symmetry occur at fields added to the domain field along the z direction:[2]

$$B_{z,AF\pm} = |h\nu/g\beta| \pm\sqrt{|B_{AZ}(2B_E + B_{AZ})|}, \quad (A2)$$

$B_{AZ}= |B_A \cos\theta|$ when $\theta= \mathbf{B_A}\wedge\mathbf{B_z}$; B_A , B_E are respectively the aligning field in a given AF domain and the field produced by an exchange interaction J_{AF} between S=1/2 states (figure 4b).

The low field, orientation dependent resonance at $B_{z,AF-}$ satisfies relation (A2) (figure 2b) for domains aligned parallel to Ta-F-Ta with g=1.74, $\sqrt{(B_E B_A)}$=170 ±10 mT and B_A = 1.7±0.1 B_E= 220 mT; B_E = 130 mT =J_{AF}=10^2 mK; $B_{z,AF+}$ is assigned to a broad ($\Delta B_{z,ms} \approx 250$ mT) in figure 2a at temperatures where (A2) is satisfied.

The exchange interaction J gives rise to the splitting of T* states above the ground singlet S (figure 5); it also determines the line shape of the D, ESR $\Delta Sz=\pm 1$ transitions according to the Anderson-Weiss theory:[5c] the shape near the center of the line, $B_{z,0}$ is Lorentzian, i.e.,

$$L' = dP_I/dB_z = C/T\ (2\pi \tau_2 \gamma)^3 B_1 (B_z-B_{z0})/[1 + (2\pi \gamma \tau_2 (B_z-B_{z0}))^2 + (2\pi \gamma)^2 \tau_2 \tau_1 B_1^2]^2,$$

C is a constant which depends on the magnetization M_0 at the temperature T, γ is the magnetogyric ratio and τ_2 is the spin-spin or transverse relaxation time. The fields of extreme slope (L" =0) occur near the center of the line in figure 2d; the increased ESR amplitude in the wings observed below T_{00} obey a Gaussian distribution function due to an increase in the second moment $<\Delta\nu^2>$ by the exchange interaction J, i.e., in the absence of saturation:[5b,c]

$$G' = dP_G/dB_z = C'/T\ (2\pi \gamma/<\Delta\nu^2>^{1/2})^3 B_1(B_z-B_{z0}) \exp(-2\pi\gamma (B_z-B_{z0}))^2/(2<\Delta\nu^2>),$$

$$d\ell n(G')/dB_z = [1 - (2\pi\gamma (B_z-B_{z0}))^2/<\Delta\nu^2>]/(B_z-B_{z0}),$$

allow for an estimate of the second moment experimentally in figure in 2d,[5b,c] then;

$$J \approx <\Delta\nu^2>/(\Delta\nu_{1/2}) \approx 15 \text{ mT (or 13 mK)} \quad (A3)$$

near T_{00}; $\Delta\nu_{1/2}/\gamma = 0.36$ mT is the half width and the slope of G' obtains $\langle\Delta\nu^2\rangle/\gamma^2 \approx 49\ mT^2$.

The T*, $\Delta S=0$, τ_1 is evaluated from the dP/dB_z amplitudes at the fields of extreme slopes, A'_{sample} relative to a reference $A'_{reference}$. In the Curie-Weiss temperature regime the ratio:

$$r \equiv (T_{sample} A'_{sample}/N_{0,sample}/B_{1,sample})/(T_{reference} A'_{reference}/N_{0,reference}/B_{1,reference})$$

$$= (1+(2\pi\gamma)^2 T_{1,reference} T_{2,reference} B_{1,reference}{}^2)^{3/2}/(1+(2\pi\gamma)^2 T_{1,sample} T_{2,sample} B_{1,sample}{}^2)^{3/2}, \quad (A4)$$

for Lorentzian lines, is determined with an accuracy of $\Delta r/r \cong 5\%$; B_1/B_{10} is known to better than 0.1% accuracy; the reference is the sample (at lowest possible B_1) checked with a free radical (1,1'bisbiphenylene2phenylallyl) at room temperature;[2,4] N_0 is the spin concentration. After confirming that $\gamma^2 T_{1,reference} T_{2,reference} B_{1,reference}{}^2 << 1$; setting $T_{1,sample} T_{2,sample} = \tau_1{}^2$ in (A4) obtains:

$$2\pi\tau_1 = (1/r^{2/3}-1)^{1/2}/\gamma B_1 \pm (2\pi\tau_1\ \Delta r/3r\ (1 - r^{2/3})^{-1}, \quad (A5)$$

in figure 4a, correct to 3 to 10 % when r=0.25 to 0.75. The saturation measurements thus give information on the T*, $\Delta S=0$ radiated levels. The population ratios are $N_{|1,-1>}/N_{|1,1>} = \exp(h\nu/k_B T_0)$ or $n_{|1,-1>}/n_{|1,1>} = \exp(h\nu/k_B T_S)$ respectively if at thermal equilibrium with the lattice and the radiation bath or when saturated at the corresponding spin temperature; the magnetization M_{T*} approaches the equilibrium value at T_0, $M_{0,T*}$ via spin-lattice and spin-spin interactions,[5b] and the chemical processes (3); the dn_i/dt for the rates given in Table I obtain the magnetization as a function of both the doublet and triplet state population of the system subject to:

$$d(n_{|1,-1>}-n_{|1,1>})/dt = -(2w^{++}n_{|1,-1>}-2w^{=}n_{|1,1>}) - (w^{+}n_{|1,-1>}-w^{-}n_{|1,1>}) - n_{|1,0>}(w^{+}-w^{-})$$
$$+ k_1\{(n_{|1/2,-1/2>})^2 - (n_{|1/2,1/2>})^2\} - k_{-1}(n_{|1,-1>} - n_{|1,1>}).$$

The half field T* most efficient relaxation rates w^{++}, $w^{=}$, w^{+} and w^{-} are induced by $h\nu_i$ phonons produced through the motion of ions carrying an electric/magnetic moment and lattice vibrational mode $q_i=2\pi\nu_i/v$ when v is the wave velocity. The magnetization relations vs T:[5b]

$$dM_{T*}/dt=(M_{0,T*}-M_{T*})/\tau_1; \quad M_{T*}= \beta N_{T*}g_{T*}(h\nu/3k_BT_{s,T*}); \quad M_{0,T*}= \beta N_{T*}\, g_{T*}\,(h\nu/3k_BT_0)$$

explain the approach to T_0 where $w^{++}-w^{=}\exp(-h\nu/k_BT_0) = w^{+}-w^{-}\exp(-h\nu/2k_BT_0) = 0$. Then assuming thermal equilibrium for the levels not at resonance with the radiation field obtains to zeroth order, a relation similar to the two level system result:[5b]

$$d(n_{|1,-1>} - n_{|1,1>})/dt = (n_{|1,-1>}+n_{|1,1>})(w^{=}-w^{++}) - (w^{=}+w^{++})(n_{|1,-1>}-n_{|1,1>}) +$$
$$+ 0.5\{(n_{|1,-1>}+n_{|1,1>}-N_{|1,-1>}-N_{|1,1>})(w^{-}-w^{+})-(n_{|1,-1>}-n_{|1,1>}-N_{|1,-1>}+N_{|1,1>})(w^{-}+w^{+})\} +$$
$$+ k_{-1}\{N_{|1,-1>} - N_{|1,1>})- (n_{|1,-1>} - n_{|1,1>})\}.$$

In the steady state approach to equilibrium, τ_1 in relation (2) obtains the working relations:

$$d(1/T_s)/dt= \{(w^{=}+w^{++}) + (w^{-}+w^{+})/2 + k_{-1}\}(1/T_0-1/T_s),$$
$$dT_{S,T*}/dt=\alpha(T_0-T_{S,T*})/C_H= (dM_{T*}/dt)/(dM_{T*}/dT_{S,T*})=(T_{S,T*}/T_0)(T_0-T_{S,T*})/\tau_1,$$
$$1/\tau_1 = (w^{=}+w^{++}) + (w^{-}+w^{+})/2 + k_{-1}. \qquad (A6)$$

$(BEDT\text{-}TTF)_3Ta_2F_{11}$

(a)

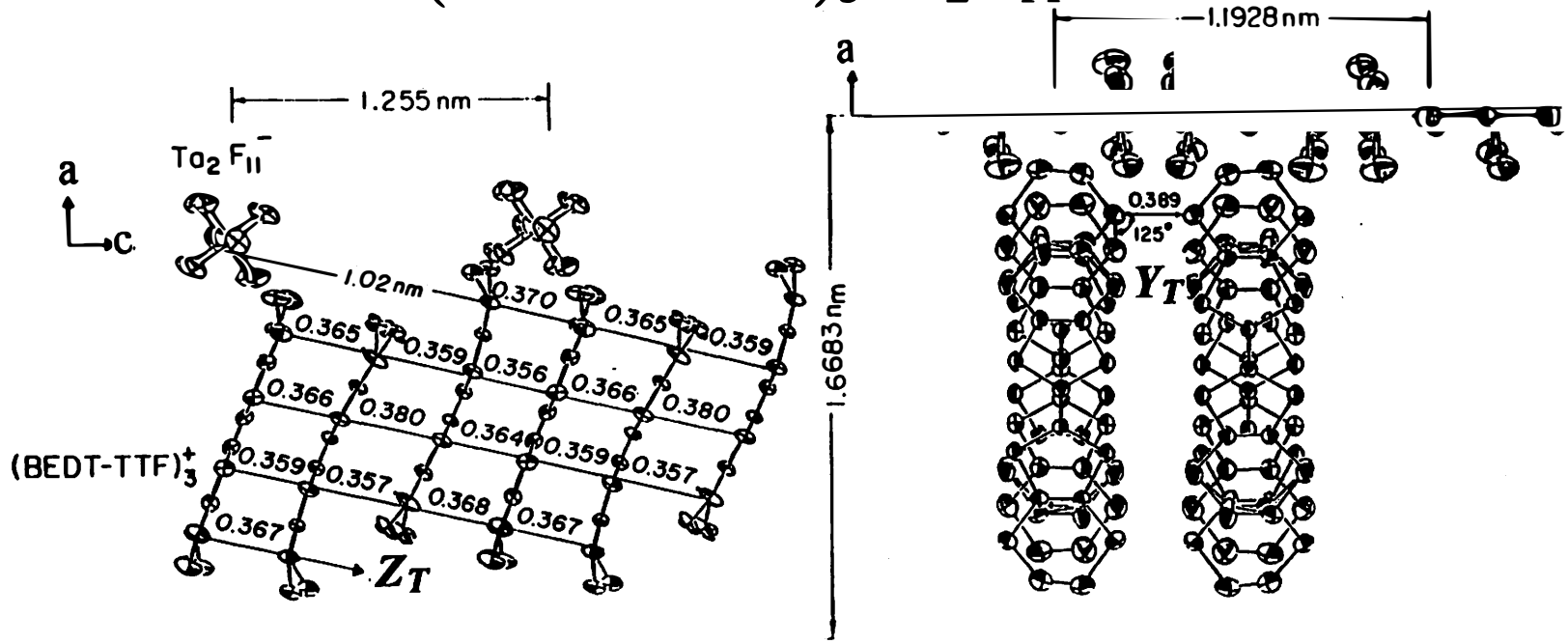

(b) Chemical Dynamics by ESR Widths

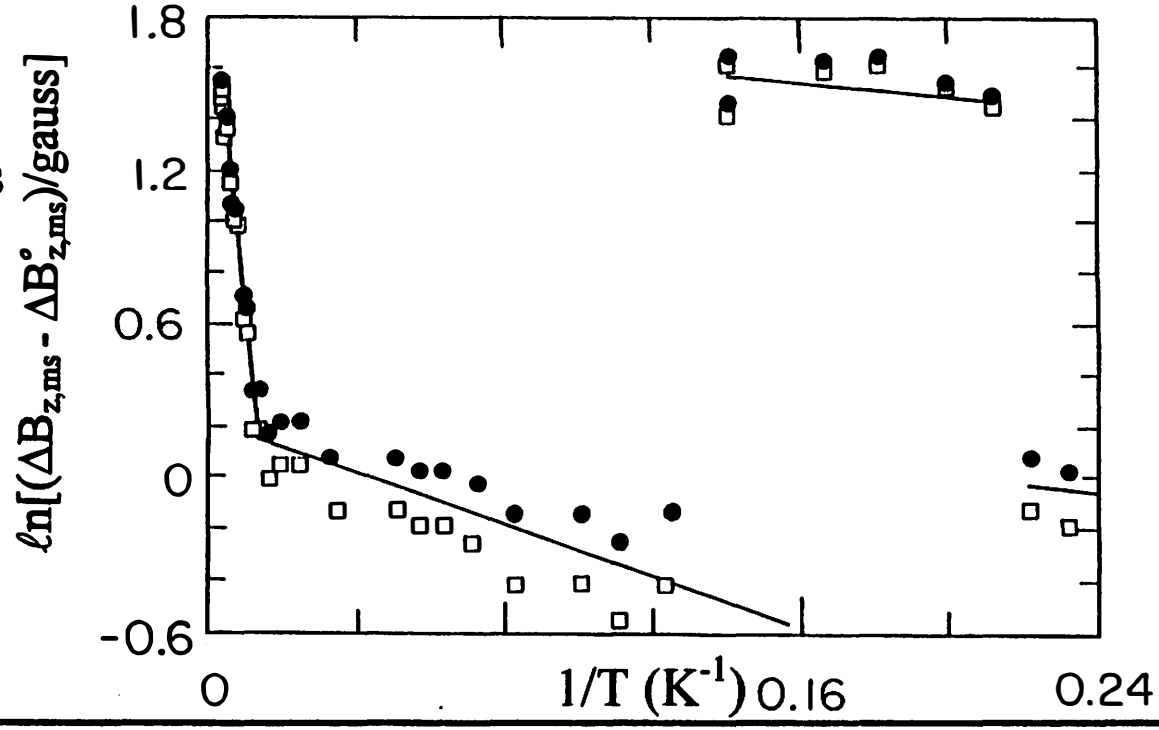

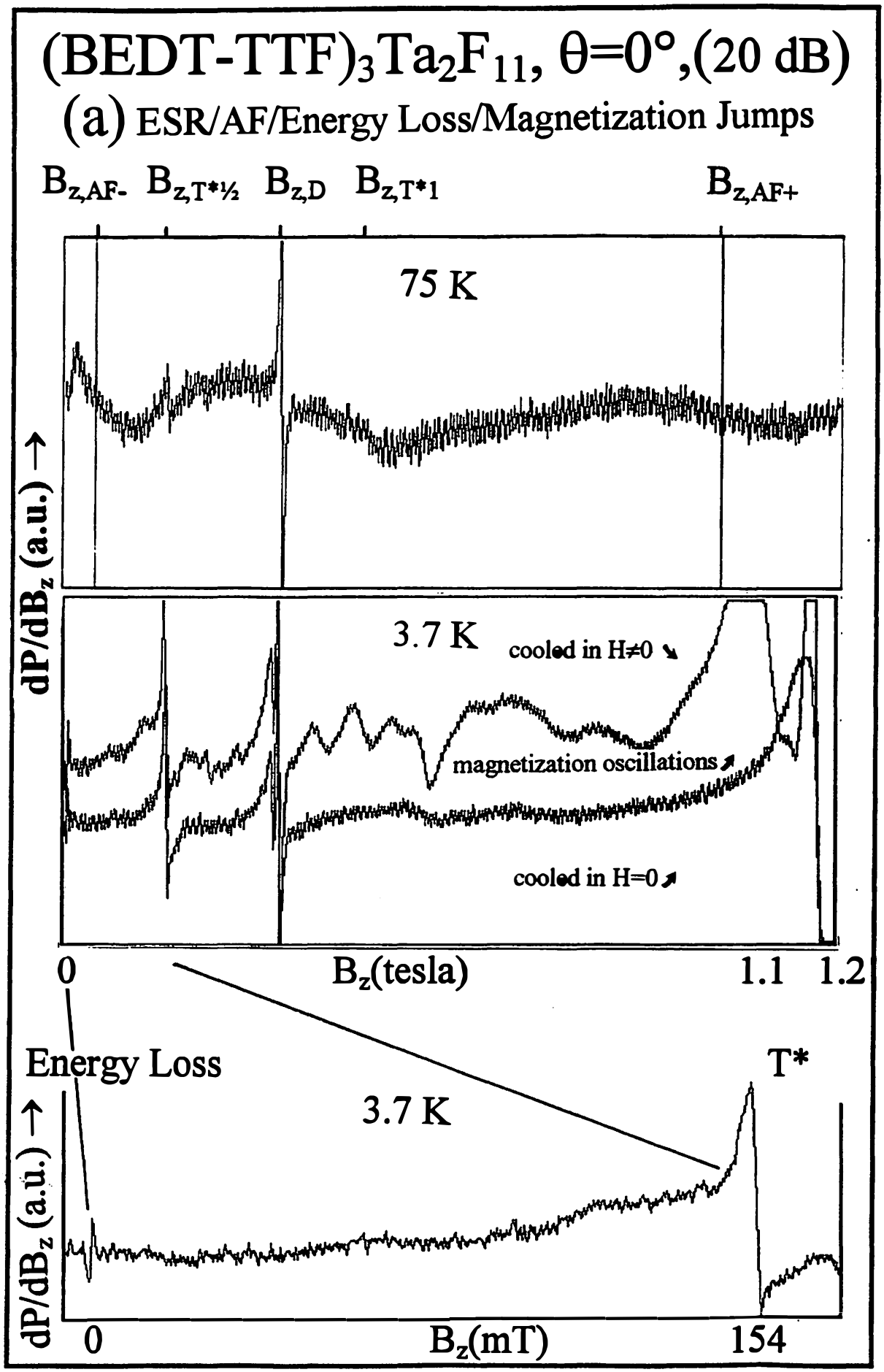
(BEDT-TTF)3Ta2F11, θ=0°,(20 dB)
(a) ESR/AF/Energy Loss/Magnetization Jumps
Bz,AF-
Bz,T*½
Bz,D
Bz,T*1
Bz,AF+
75 K
3.7 K
cooled in H≠0
magnetization oscillations
cooled in H=0
dP/dBz (a.u.) →
0
Bz(tesla)
1.1
1.2
Energy Loss
T*
3.7 K
dP/dBz (a.u.) →
0
Bz(mT)
154

Fig 2b

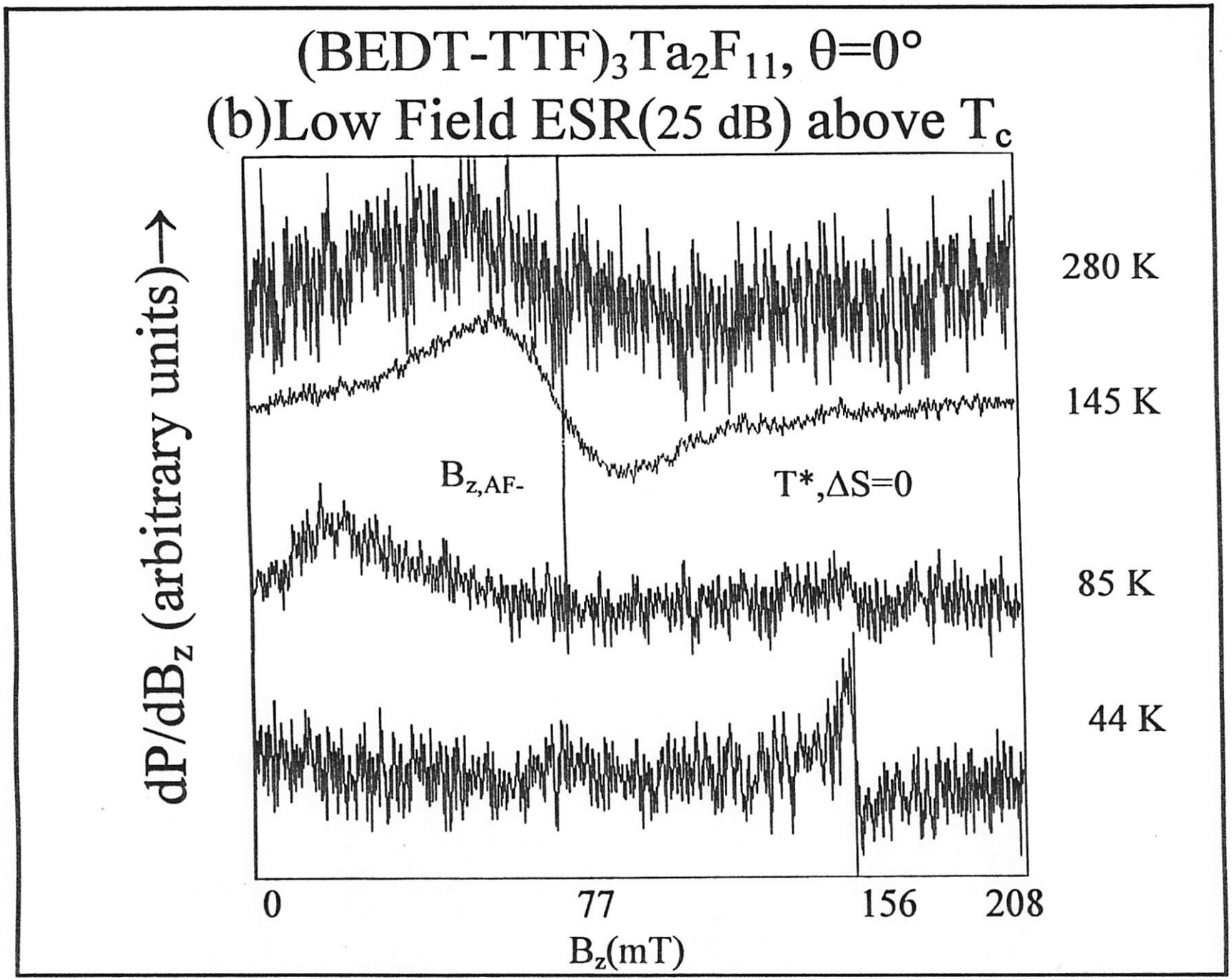
(BEDT-TTF)3Ta2F11, θ=0°
(b)Low Field ESR(25 dB) above Tc
dP/dBz (arbitrary units)→
280 K
145 K
85 K
44 K
Bz,AF-
T*,ΔS=0
0
77
156
208
Bz(mT)

$(BEDT\text{-}TTF)_3Ta_2F_{11}$, θ=20°, 3.7K ESR

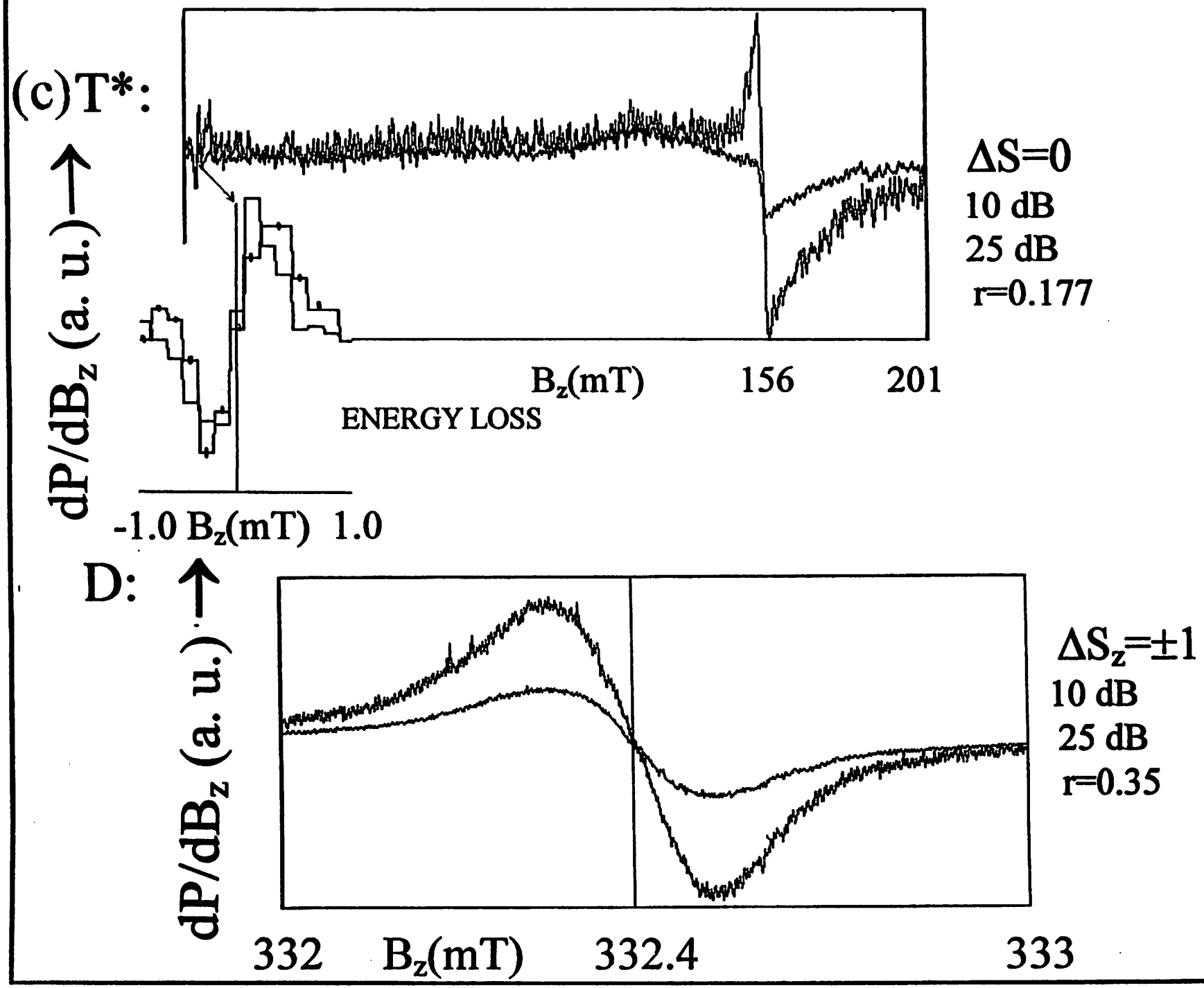

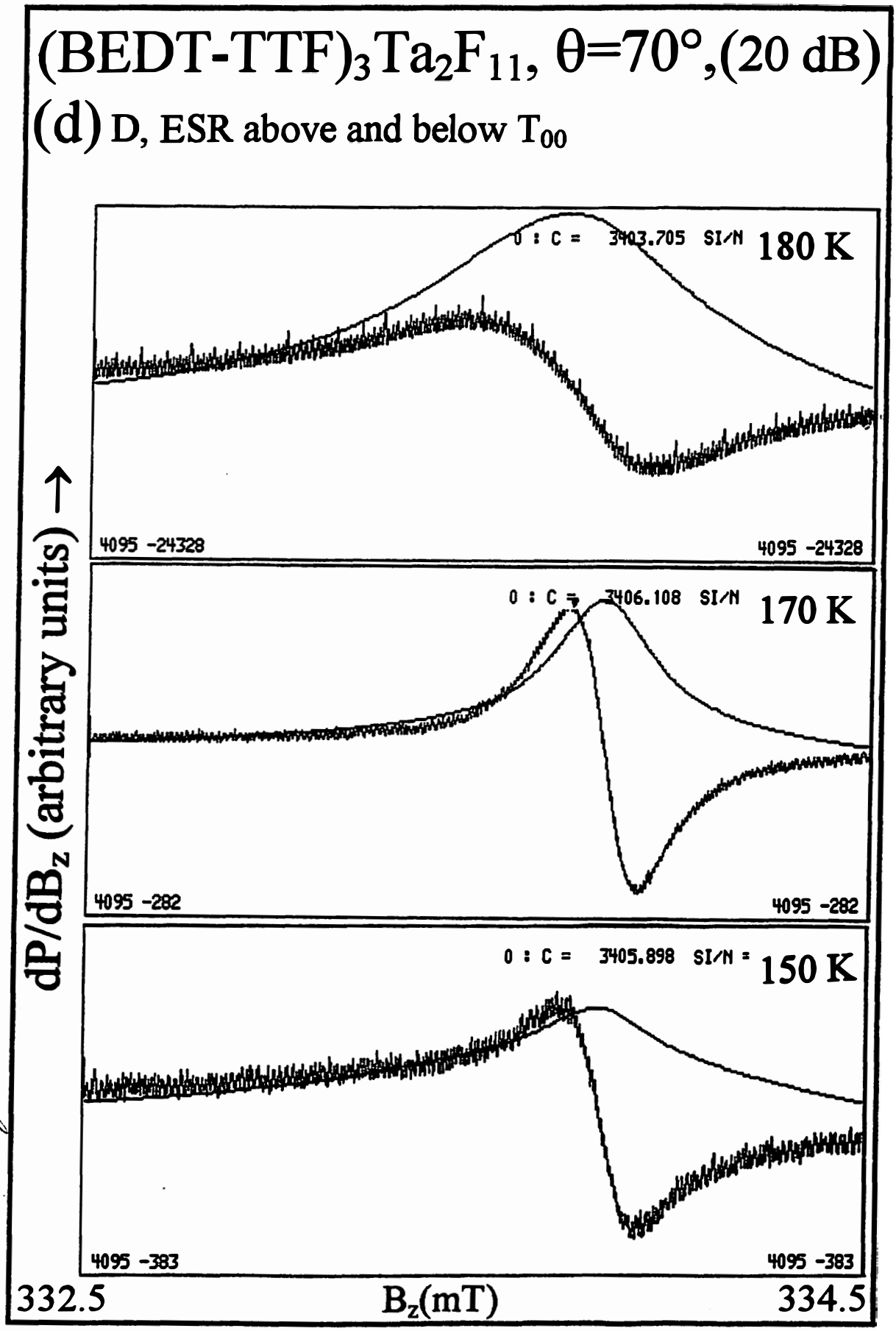
(BEDT-TTF)3Ta2F11, θ=70°,(20 dB)
(d) D, ESR above and below T00
0 : C = 3403.705 SI/N
180 K
4095 -24328
4095 -24328
0 : C = 3406.108 SI/N
170 K
4095 -282
4095 -282
0 : C = 3405.898 SI/N
150 K
4095 -383
4095 -383
dP/dBz (arbitrary units) →
332.5
Bz(mT)
334.5

Fig 2d

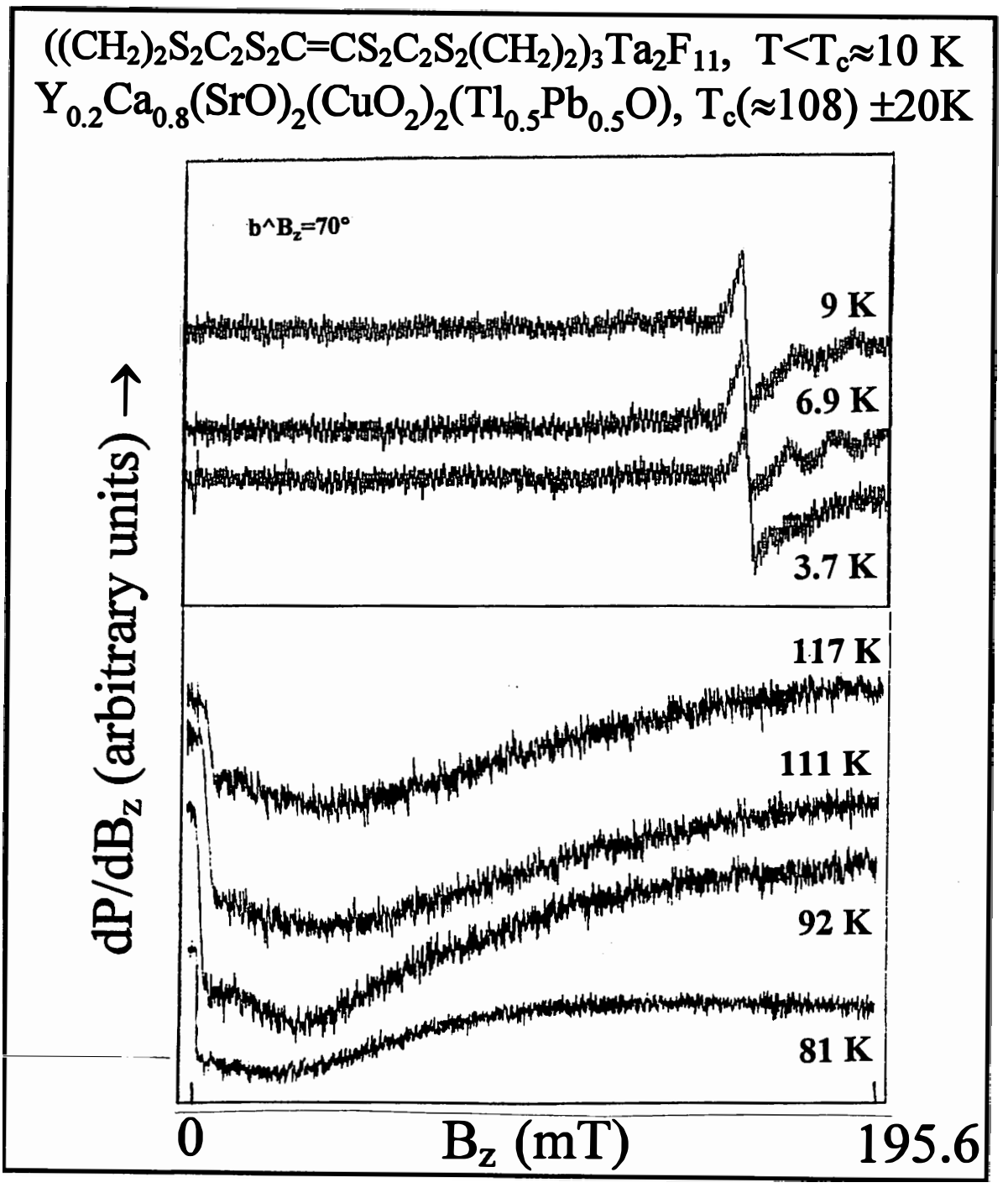
((CH2)2S2C2S2C=CS2C2S2(CH2)2)3Ta2F11, T<Tc≈10 K
Y0.2Ca0.8(SrO)2(CuO2)2(Tl0.5Pb0.5O), Tc(≈108) ±20K
b^Bz=70°
9 K
6.9 K
3.7 K
117 K
111 K
92 K
81 K
dP/dBz (arbitrary units) →
0
Bz (mT)
195.6

$(BEDT\text{-}TTF)_3Ta_2F_{11}$ Energy Level Diagram in $B_{z,1/2}$

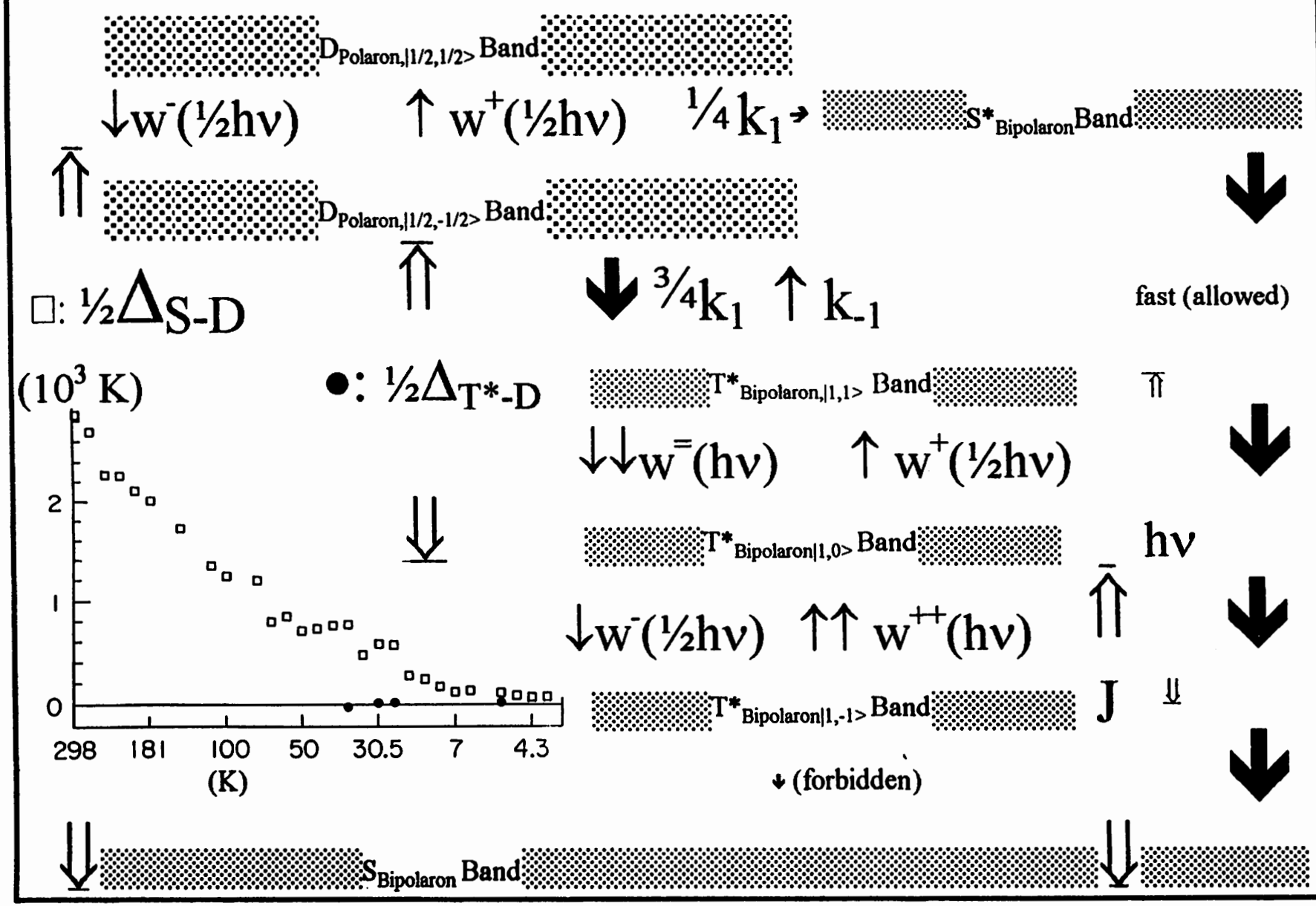

Fig 5

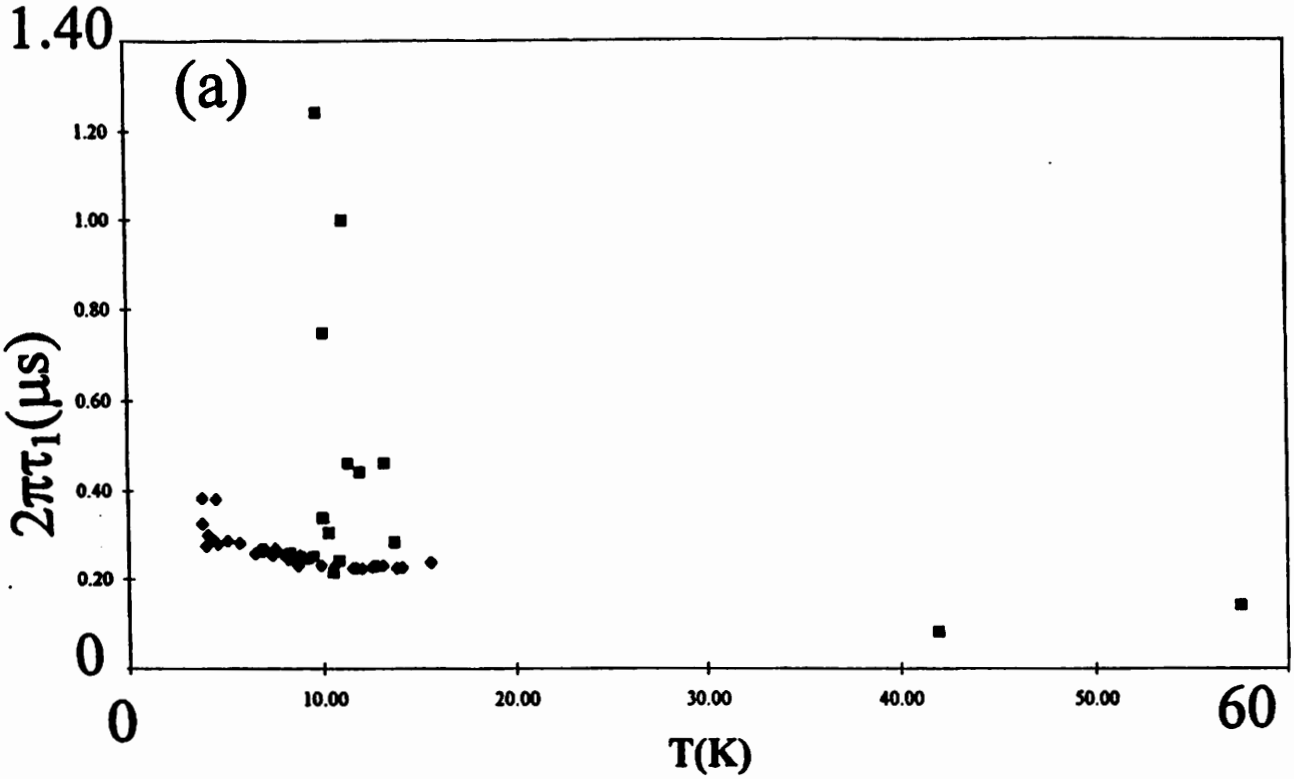
(a)
1.40
1.20
1.00
0.80
0.60
0.40
0.20
0
$2\pi\tau_1(\mu s)$
0
10.00
20.00
30.00
40.00
50.00
60
T(K)

Fig a

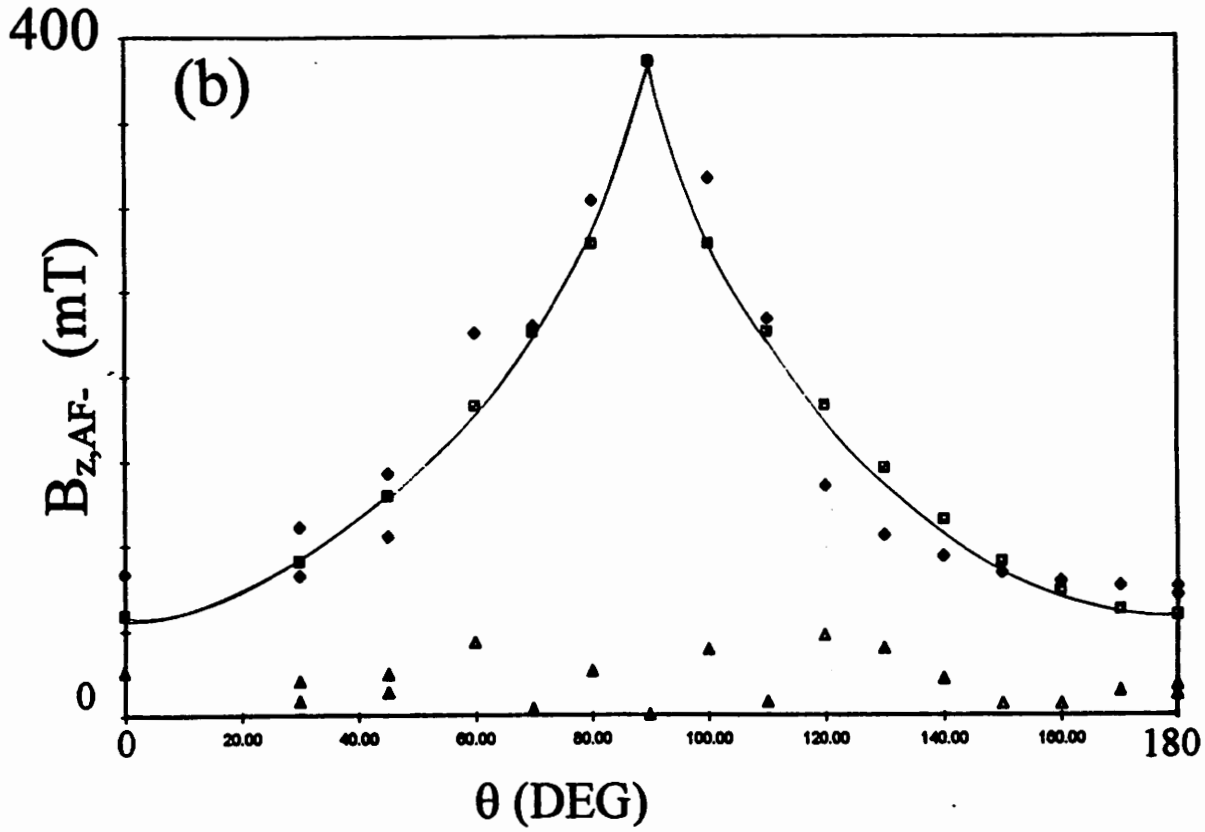
(b)
400
0
$B_{z,AF-}$ (mT)
0
20.00
40.00
60.00
80.00
100.00
120.00
140.00
160.00
180
θ (DEG)

Fig 2b